

Electronic Supporting Information

Engineering light-driven micromotors with fluorescent dye coatings for easy detection and tracking

Srikanta Debata, Suwendu Kumar Panda, and Dhruv Pratap Singh*

Department of Physics, IIT Bhilai, Kutelabhata, Durg, Chattisgarh, 491001, India.

*Corresponding Author: dhruv@iitbhilai.ac.in

1. Guide to supplementary Videos

Video S1: Video shows fluorescent signals identification of the active motion as well as the position of micromotors in 2.5 % conc. of peroxide medium under low-intensity UV light and visible light irradiation. The playback speed is 2X.

Video S2: Video shows the fluorescent signaling of active swimming of micromotors through low-intensity visible light irradiation in 2.5% conc. of peroxide medium. The playback speed is 2X.

Video S3: Video shows that fluorescent emission helps to differentiate the moving micromotors from the similar size immovable bacteria entities in 2.5 % conc. of peroxide medium under low-intensity visible light irradiation. The playback speed is 2X.

Video S4: Video shows that fluorescent emission and motility helps to detect the active micromotors in a complex media containing stray fluorescent objects in 2.5 % conc. of peroxide medium under low-intensity visible light irradiation. The playback speed is 2X.

Video S5: Video shows the importance of fluorescent signals for determining the shape and direction of propulsion of rod-structured micromotors under low-intensity UV light irradiation. The playback speed is 2X.

2. Supplementary figure description

2.1 XRD analysis

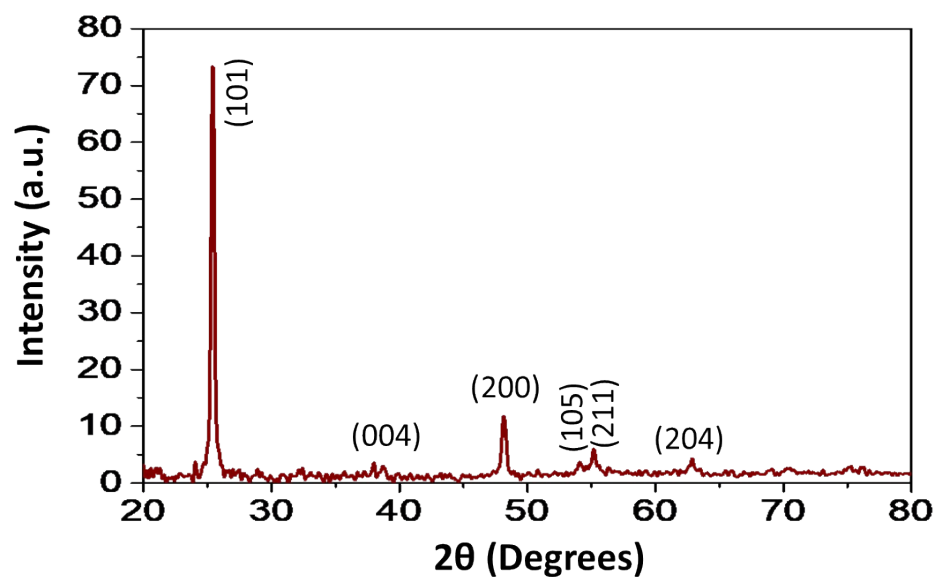


Fig. S1 The X-ray diffraction (XRD) plot shows the crystalline anatase phase of TiO₂.

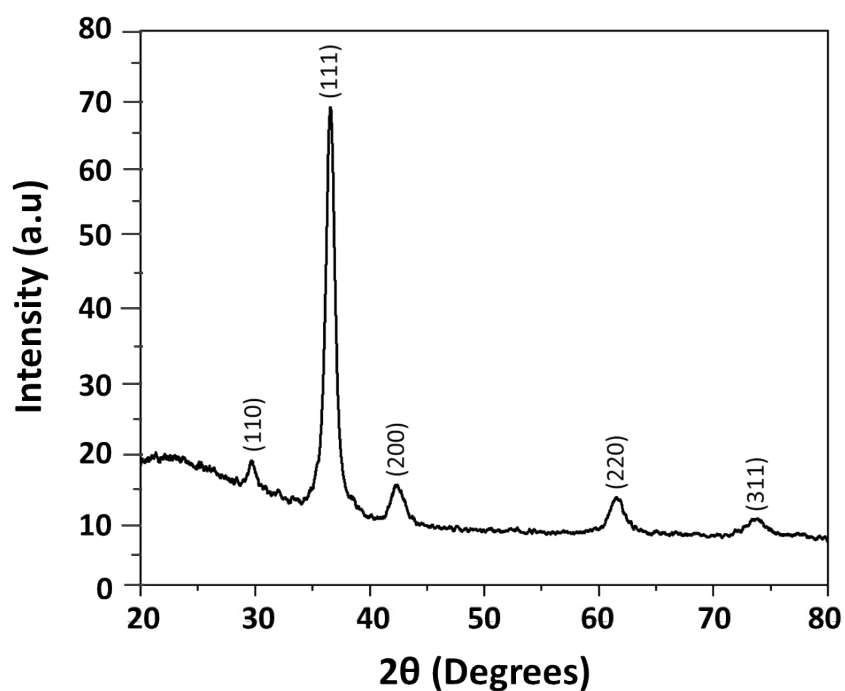


Fig. S2 The X-ray diffraction (XRD) plot shows the diffraction peaks to ensure the formation of Cu₂O.

2.2 Fluorescence emission spectra of different dyes

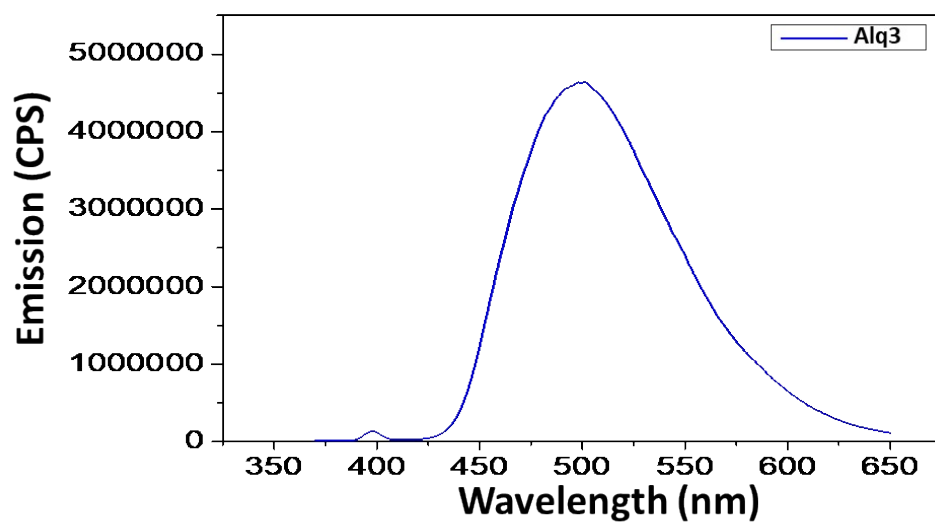


Fig. S3 Fluorescent emission spectra show the broad fluorescent emission peak of the Alq3 dye with the excitation around 360 nm.

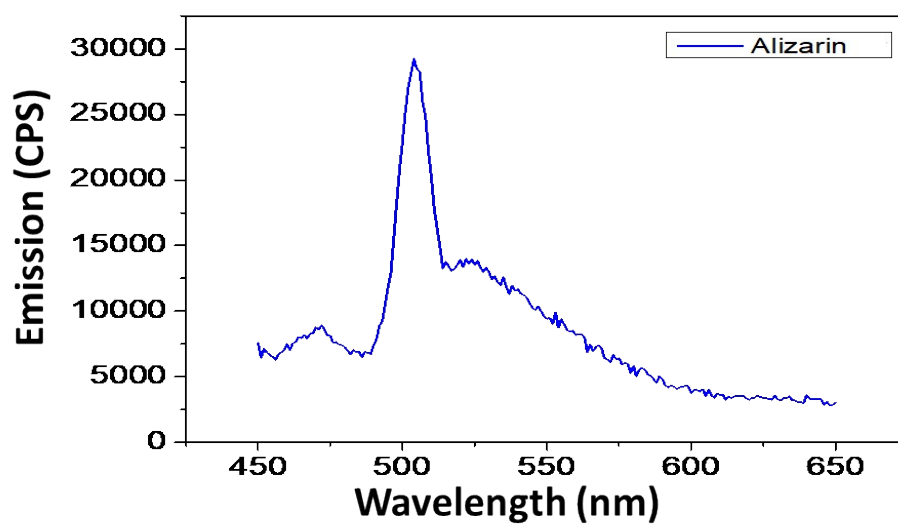


Fig. S4 Fluorescent emission spectra show the broad fluorescent emission peak of the Alizarin dye with the excitation around 430 nm.

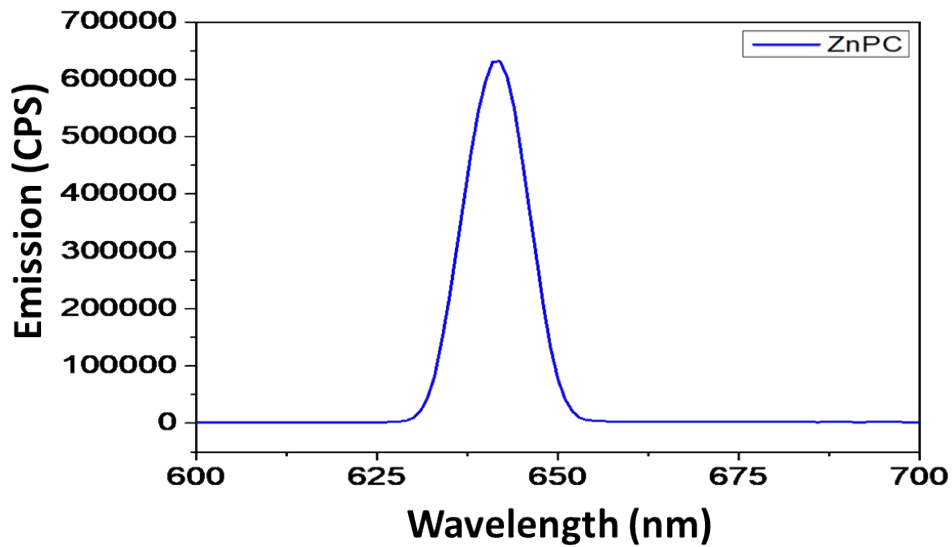


Fig. S5 Fluorescent emission spectra show the broad fluorescent emission peak of the Zinc phthalocyanine (ZnPC) dye with an excitation around 340 nm.

2.3 Fluorescence based motion detection of Cu_2O -based micromotors

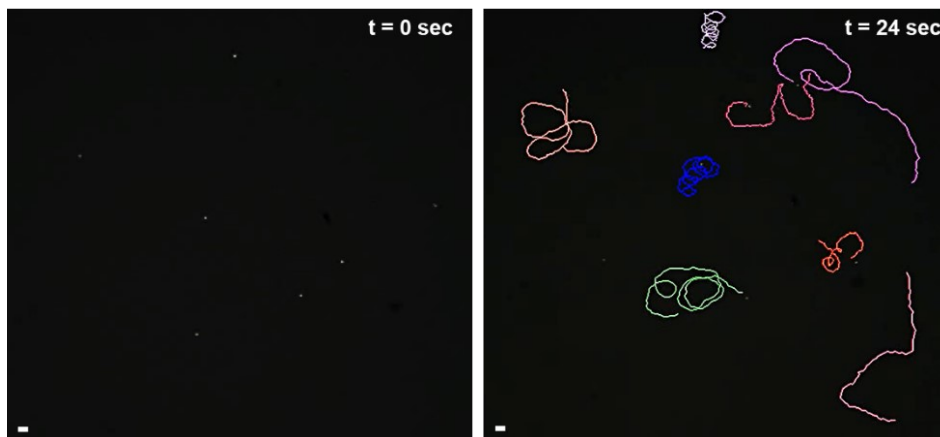


Fig. S6 Fluorescent images of Cu_2O based dye coated micromotor under UV light irradiation at time 0 sec and 24 sec respectively. Scale bar is 5 μm .

3. Rationales of dye selection

There are some rationales for choosing the specific dyes, such as:

- a. The dye was chosen for its powder form and low melting point, making it suitable for deposition via physical vapor deposition (PVD) techniques.
- b. Good fluorescence response.

- c. Finally, the dyes were selected based on their excitation and emission wavelength ranges. Alq3 dye excites under UV light and emits in the green wavelength, Alizarin excites and emits in the visible light region, and ZnPC excites under UV light and emits in the red wavelength. These specific properties make the dyes effective for detecting motion and position, as well as determining the shape and propulsion direction of the micromotors.

4. Code information for tracking the micromotors

A python code is used for tracking micromotors, and it is based on a CSRT tracker provided in the Open-Source Computer Vision Library. The detailed discussion about tracking algorithms is given as follows:

- A. Initially, the associated libraries such as OpenCV (cv2) and NumPy are imported for image processing and calculation.
- B. Tracking of micromotors:
 - a. Capture video: Opens the video file using `cv2.VideoCapture`.
 - b. Initialize tracker: Creates a CSRT tracker using `cv2.TrackerCSRT_create()`.
 - c. Select ROI: Implementation of a method to select the initial bounding box of the microrobot on the first frame (e.g., using `cv2.selectROI`) is needed.
 - d. Tracking loop:
 - i. Reads each frame from the video.
 - ii. Updates tracker position with `tracker.update`.
 - iii. Draws bounding box on the frame.
 - iv. Displays the frame.
- C. After tracking the micromotors in X-Y plane, the position coordinate (x and y coordinates data) for each frame can be exported to an Excel supported CSV file. From the X, Y coordinates data and knowing the frames captured per second data, the speed can be calculated by using the mathematical formula.

5. Limitation of the code's capabilities

The code accurately tracks time data by determining the frames per second (fps) using the `cv2.CAP_PROP_FPS` command. Based on the recorded fps, it calculates the time intervals

between frames. For example, if a video is recorded at 20 fps, the code tracks each consecutive frame with a 0.05-second interval. In our experiment, videos were captured at 10–20 fps, which the code successfully detected. According to our understanding, the code can handle higher frame rates, such as 50–100 fps, as it directly extracts fps from the video.

The minimum time interval the code can detect is approximately 100 fps, corresponding to a 0.01-second time difference between frames. The upper limit for tracking is only constrained by the storage capacity of the computer, allowing it to handle videos up to several hours in length, though larger data files will require significant storage space. Moreover, the code can track particles of the same size as those visible in the captured video. Particles with sizes in the range of 200–300 nm typically appear as points in high-magnification recorded video, which this Python code can track. Below this size limit, live imaging through optical microscope is not possible. Therefore, the code is capable of tracking particles ranging in size from approximately 0.2–0.3 μm to several centimetres.

6. Behavior of micromotors before and after dye coating

The thin layer of the dyes upon the titania surface of the micromotors does not significantly contribute to the enhancement of speed of micromotors. We agree that there is a possibility of electron transfer between the dye molecules and the semiconductor, however, it requires specific conditions, such as proper alignment of the optical energy bands between the dye and semiconductor. Additionally, any changes in optical absorption intensities should occur with the dye coating. To explore potential interactions between the dye and semiconductor, we thoroughly characterized the micromotors using recommended parameters. UV-vis spectroscopy (Fig. S7) showed that the absorption spectra before and after dye coating were nearly identical, indicating no notable change in the optical properties and no significant interaction between the dye molecules and the semiconductor. Furthermore, we measured the speed of the micromotors before and after dye coating under maximum UV light intensity in a 2.5% peroxide medium. The speeds were $2.95 \pm 0.3 \mu\text{m s}^{-1}$ before coating and $2.74 \pm 0.4 \mu\text{m s}^{-1}$ after coating, demonstrating no significant change, likely due to the extremely thin dye layer.

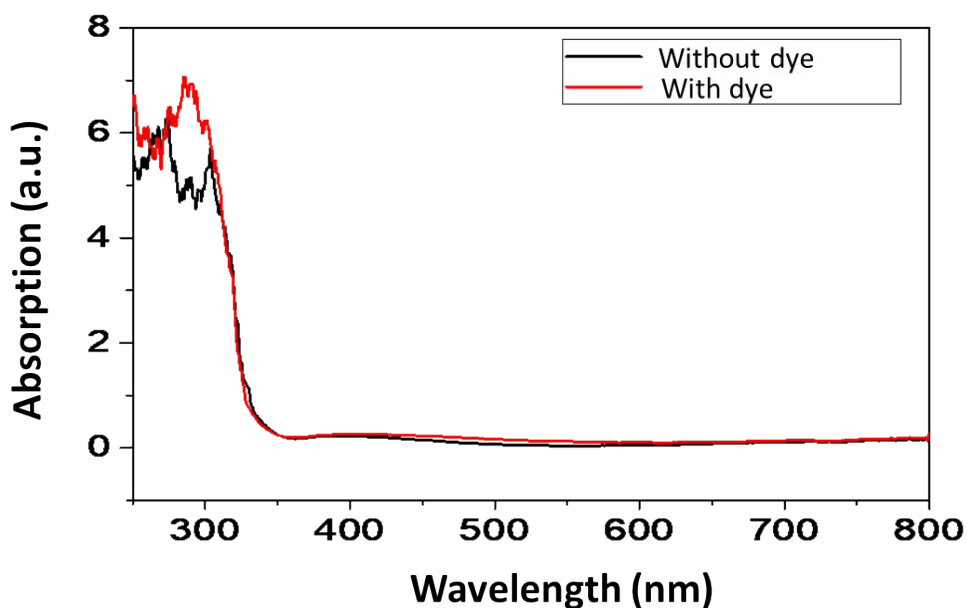


Fig. S7 UV-vis absorption spectroscopy of micromotors without and without dye coating.

7. Swimming speed of micromotors

7.1 Depending on the fuel concentration

We have optimized the fuel concentrations and included the graph shown below (Fig. S8). The rationale for selecting 2.5% (v/v) H_2O_2 is that this concentration provided the optimal speed for the micromotors. Beyond this concentration, the speed became saturated with no further increase. Therefore, a relatively lower fuel concentration of 2.5% (v/v) was chosen for all experiments.

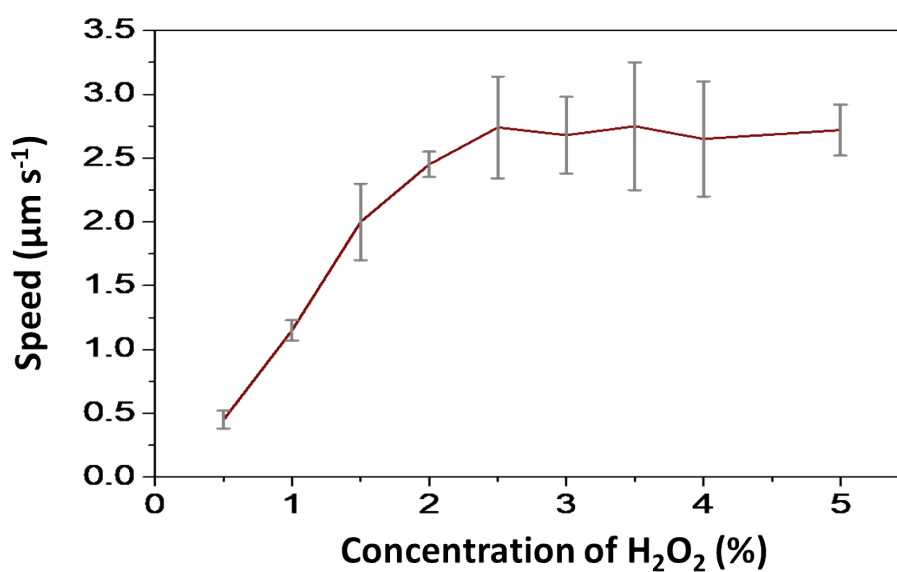


Fig. S8 Concentration of peroxide fuel (in %) vs speed graph of the TiO₂ based dye coated micromotors.

7.2 Depending on the light intensity

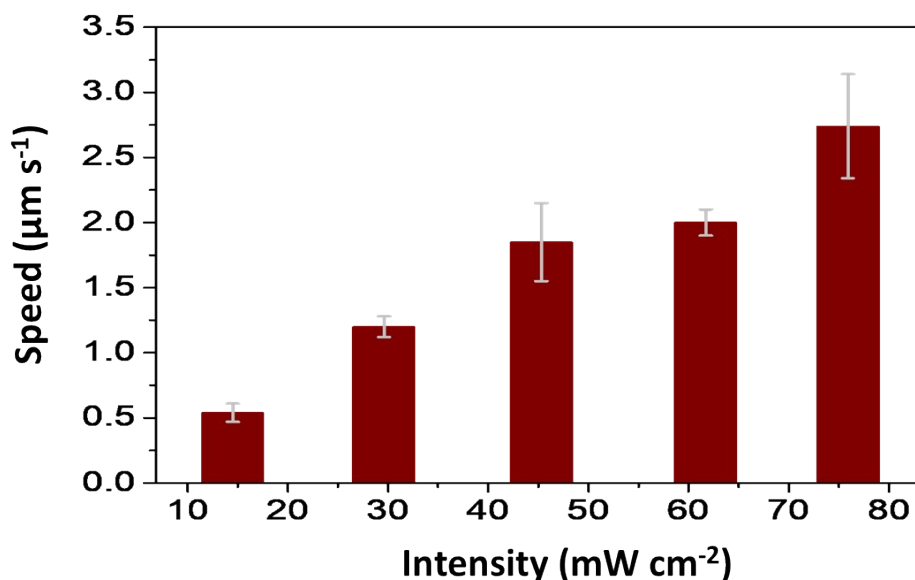


Fig. S9 Light intensity vs speed graph of the TiO₂ based dye coated micromotors in 2.5% H₂O₂ medium.

8. Fluorescence stability of micromotors

To verify fluorescence quenching, we exposed the dye-coated micromotors to UV light for an extended period in a 2.5% (v/v) peroxide medium. Time-lapse images were captured at various intervals during the exposure. From the images, we observed minimal or negligible quenching of the fluorescence signal, even after 1 hour of continuous exposure, and the fluorescence emission remained quite stable. Therefore, we believe this stability is sufficient for real-time applications of dye-coated micromotors. Additionally, since the chosen dyes have different excitation and emission wavelengths, no significant cross-talk between the dye molecules was detected. The time-lapse images are shown in Fig. S10.

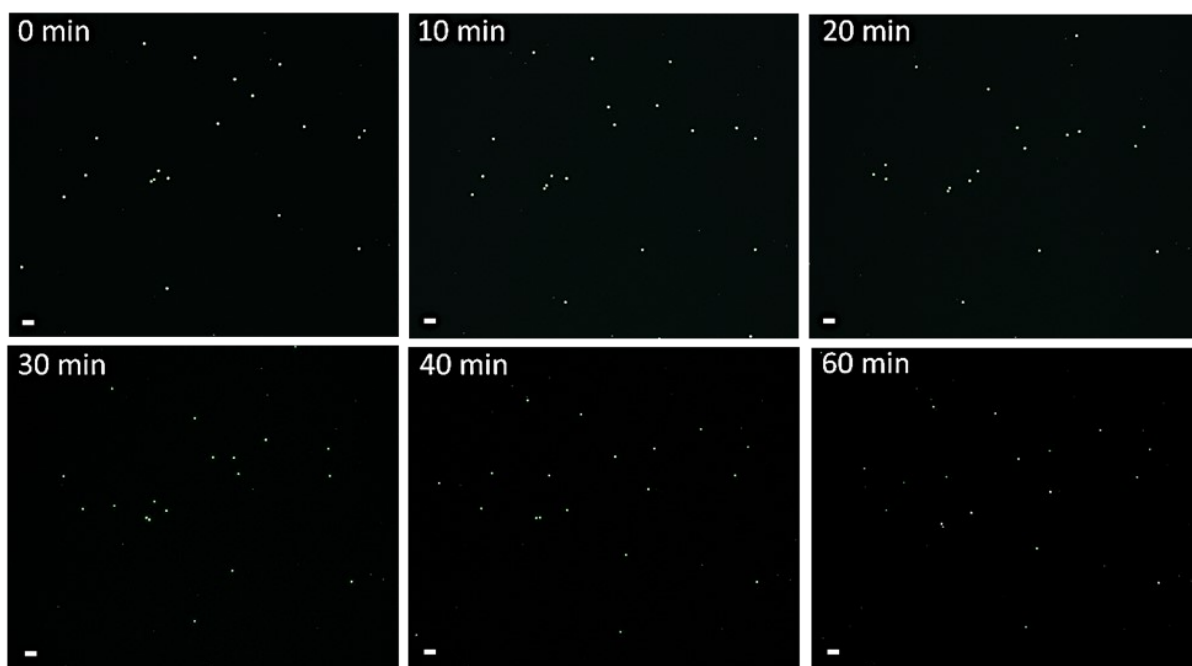


Fig. S10 The fluorescence images of the dye-coated micromotors, captured at different time intervals under prolonged UV light exposure, demonstrate the stability of the fluorescence signal. The scale bar is 10 μm .

9. Mechanism of fluorescence emission by dye molecules

Fluorescence is one of the most important and extensively used techniques in physiology, cell biology, and even in clinical medicine. Moreover, fluorescence is a photoluminescence phenomenon, where the light is emitted from an electronically excited state of a populated state upon external excitation. The mechanism behind the fluorescence can be understood from the Jablonski diagram.^{1,2} When a fluorescent particle absorbs a quantum of light energy (photon), the electrons in an ion, atoms, or molecules get excited and jump to the higher energy state from the ground state. The absorption of light is a radiative process where the electrons from the singlet spin state S_0 jump to the higher excited state S_2 through an internal transition as shown in Fig. S11. The transition of the electron is represented by blue arrows which is the fastest transition throughout the Jablonski diagram, that occurred in femtoseconds. At ambient temperature, the maximum no. of electrons in an atom or a molecule exists in the lowest vibrational energy phase of the ground state, and therefore the absorption of energy begins from there. The transition can be seen in Fig. S11, that the electrons are jumping from the singlet S_0 level to one of the vibrational states of singlet excited levels. After reaching the excited state, the molecule stays in a non-equilibrium state

and eventually returns to the ground state after dissipating the gained energy. The primary stage for energy loss is through non-radiative vibrational relaxation with either intramolecular or intermolecular transitions. The time scale for vibrational relaxation is around a few Pico to a few Angstrom seconds. Another way of non-radiative energy loss is through internal conversion where a molecule undergoes a transition from the higher-lying spin singlet state to the lower-lying spin singlet state ($S_2 \rightarrow S_1$). The internal conversion immediately takes place after the completion of vibrational relaxation. The internal conversion rate is inversely proportional to the gap of energy between two electronic states and the time scale for it to happen is around 10^{-11} to 10^{-9} sec. In contrast, the gap in energy between the S_1 state and the S_0 state is much wider, and the rate of internal conversion is very small. So, a radiative transition in molecules occurs from the same spin state of the S_1 state to the S_0 state, through a process known as fluorescence. The time scale for fluorescence transition is around 10^{-10} to 10^{-7} sec and can be seen through the orange arrows in Fig. S11. Due to the continuous internal conversion and vibrational relaxation processes, the fluorescence emission from the S_1 state to the S_0 state loses its energy as compared to the absorbed energy by the ground electronic state for a molecular transition. Subsequently, energy loss leads to a shifting in the wavelength of light between absorption and emission, which is known as Stoke's shift as shown in Fig. S12. Therefore, a fluorescent particle always emits a wavelength of light higher than that of an absorbed light. From the Jablonski diagram and Stoke's shift, it is clear that the fluorescence emission occurs instantly after a passage of events and there is an energy loss between the emission and absorption transition. After understanding the whole fluorescent nature, the multiple dyes coated micromotors were used for some interesting studies.

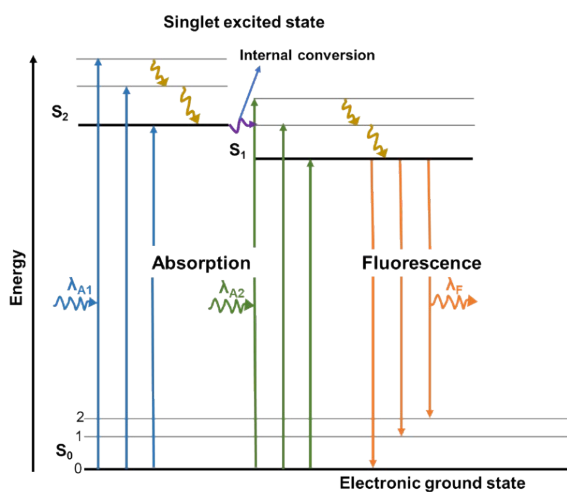


Fig. S11 Jablonski's diagram.

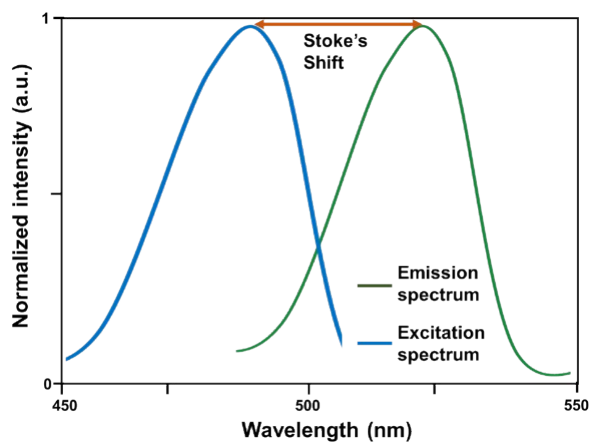


Fig. S12 Stoke's shift.

References:

- 1 Z. Limpouchová and K. Procházka, in *Fluorescence Studies of Polymer Containing Systems*, ed. K. Procházka, Springer International Publishing, Cham, 2016, vol. 16, pp. 91–149.
- 2 H. Chen, L. Liu, K. Qian, H. Liu, Z. Wang, F. Gao, C. Qu, W. Dai, D. Lin, K. Chen, H. Liu and Z. Cheng, *Sci. Adv.*, 2022, **8**, eabo3289.